A Local Approach for Inter-individual Functional Registration

Isabelle Corouge, Pierre Hellier, Bernard Gibaud, Christian Barillot

INRIA

INSTITUT NATIONAL DE RECHERCHE EN INFORMATIQUE ET EN AUTOMATIQUE

A Local Approach for Inter-individual Functional Registration

Isabelle Corouge , Pierre Hellier , Bernard Gibaud , Christian Barillot

N°4415

Mars 2002

THÈME 3

ISSN 0249-6399 ISRN INRIA/RR--4415--FR+ENG

A Local Approach for Inter-individual Functional Registration

Isabelle Corouge , Pierre Hellier* , Bernard Gibaud † , Christian Barillot ‡

Thème 3 — Interaction homme-machine,
images, données, connaissances
Projet Vista

Rapport de recherche n ° 4415 — Mars 2002 — 27 pages

Abstract: Within the scope of three-dimensional brain imaging, we propose an inter-individual fusion scheme to register functional activations according to anatomical cortical structures, the sulci. This paper is based on the assumption that an important part of the functional inter-subject variability is encoded in the anatomical variability. Therefore, we aim in this paper at proposing a generic framework to register functional activations according to relevant anatomical landmarks. Compared to "classical" inter-individual fusion schemes, this approach is local. It relies on a statistical sulci shape model accounting for the inter-individual variability of a population of subjects, and providing deformation modes relatively to a reference shape (a mean sulcus). The deformation field obtained between a given sulcus and the reference sulcus is extended to a neighborhood of the given sulcus by using the thin-plate spline interpolation. It is then applied to functional activations located in the vicinity of this sulcus. This approach is compared with rigid and non rigid registration methods. We present in this paper results on MEG somatosensory data acquired on 18 subjects. We show that the non-linear local fusion scheme significantly reduces the functional variability after registration.

Key-words: 3D cerebral imaging, probabilistic neuroimaging atlas, statistical shape model, thin-plate spline, non-linear registration, cortical sulci, functional activations, MEG dipoles.

(Résumé : tsvp)

* IRISA-INRIA,{icorouge,phellier}@irisa.fr
† Laboratoire IDM, Université de Rennes 1, bernard.gibaud@univ-rennes1.fr
‡ IRISA-CNRS, cbarillo@irisa.fr

Unité de recherche INRIA Rennes
IRISA, Campus universitaire de Beaulieu, 35042 RENNES Cedex (France)
Téléphone : 02 99 84 71 00 - International : +33 2 99 84 71 00
Télécopie : 02 99 84 71 71 - International : +33 2 99 84 71 71

Une approche locale pour le recalage inter-sujets de données fonctionnelles

Résumé : Dans le cadre de l'imagerie cérébrale tridimensionnelle, nous proposons un schéma de fusion inter-individuelle pour recaler des activations fonctionnelles selon des structures anatomiques corticales, les sillons. Ce schéma est basé sur l'hypothèse qu'une part importante de la variabilité inter-sujets fonctionnelle est encodée sur la variabilité anatomique. Notre objectif est de proposer un cadre générique pour recaler des activations fonctionnelles selon des amers anatomiques pertinents. Comparée à des approches "classiques" de fusion inter-individuelle, notre approche est locale. Elle s'appuie sur un modèle statistique de formes des sillons rendant compte de la variabilité inter-individuelle d'une population de sujets, et forunissant des modes de déformation par rapport à une forme de référence (un sillon moyen). Le champ de déformation obtenu entre un sillon donné et le sillon de référence est étendu à un voisinage local du sillon donné en utilisant l'interpolation basée sur les thin-plate splines. Il est alors appliqué aux activations fonctionnelles localisées au voisinage de ce sillon. Cette approche est comparée à des méthodes de recalage rigide et non-rigides. Nous présentons des résultats obtenus sur des données somesthésiques acquises par MagnétoEncéphalo-Graphie (MEG) sur 18 sujets. Nous montrons que le schéma de fusion inter-individuelle non-linéaire local réduit de façon significative la variabilité fonctionnelle après recalage.

Mots-clé : Imagerie cérébrale 3D, atlas probabiliste, modèle statistique de formes, thin-plate spline, recalage non-linéaire, sillons corticaux, activations fonctionnelles, dipôles MEG.

1 Introduction

In the context of inter-individual normalization, we address in this paper the registration of 3D anatomical and functional data, *i.e.* data from various subjects and acquired with various modalities (e.g. magnetic resonance imaging (MRI) for anatomical data, magnetoencephalography (MEG) or functional magnetic resonance imaging (fMRI) for functional data, *etc* ...). While anatomical imaging visualizes brain morphology, tissues, *etc* ... , functional imaging enables to localize cerebral activity. They thus provide complementary information which can be exploited to give a functional cartography of human brain, or to construct anatomical and functional atlases [7], [18], [25]; such atlases being particularly expected to account for the inter-individual variability. Assuming that an important part of the functional inter-subject variability is encoded on the anatomical variability, the proposed method intends to express functional multi-patients data in a single referential linked to an anatomical model.

Inter-subject registration techniques abound in literature [16]. Global methods aim at finding a transformation registering one volume toward another one, most of them by optimizing a similarity measure between the two volumes. When based on luminance information, this similarity criterion offers the advantage to take into account all available information, but easily fails in regions like cortical areas where the inter-individual variability is high [11]. That's why methods which explicitly exploit anatomical information by registering particular anatomical structures are attractive. However they often lack a sufficient number of landmarks to handle the high inter-individual variability issue. Accordingly, a powerful tool to image analysis like active shape models (among which we will retain only those leading to a modal analysis) is an appealing alternative [19], since such models are not only able to represent the shape of an object but also the way it can vary. Either they rely on a physical [23], [17], or on a statistical [13], [5], approach, they require a learning stage, achieved thanks to a training set, to perform the adequation between model and data, and by this mean are able to capture the variability within a class of objects. Although shape models are generally used for segmentation purpose, we have investigated in this paper their use in the context of anatomo-functional normalization, to register sparse data associated with the modeled structures of interest.

With this goal, we propose a registration method which is both local and based on a cortical sulci shape model. It relies on the assumption that sulci are relevant anatomical landmarks for functional analysis [27]. The registration of functional data, which are located in a spatial neighborhood of cortical sulci, is finally achieved thanks to a technique based on the thin-plate spline interpolation [1], [2].

In Sect. 2, we describe the construction of the statistical model of cortical sulci, performed by learning from a set of shapes. The training stage is first detailed, then we present the statistical analysis method, *i.e* a principal component analysis (PCA). In Sect. 3 we introduce the interpolation scheme and the way it can be combined to the statistical shape model for the local and non-linear registration of functional activations. Then the performance is illustrated on experimental MEG somatosensory data. We compare this approach with a local rigid registration approach and with global registration methods (rigid and non-rigid).

2 Statistical Model of Cortical Sulci

Cortical sulci are anatomical structures whose shape variations among individuals are complex. We propose to build a model of these structures from a statistical analysis of a training set in order to result in a compact and meaningful representation of their shapes and of their variations. However, using a statistical analysis implies some constraints. It requires particularly to establish the point to point correspondences of the shapes to learn, in the sense that the parameter-vectors representing the data have to correspond. Therefore, the training stage needs to consider the following points: the extraction of the structures of interest, their representation and their matching.

2.1 Training

The extraction and representation of the cortical sulci used in this paper result from previous work [15], [9], which we briefly recall now. Sulci are defined as their median surface and extracted from MRI volumes by a method now known as the "active ribbon" method which leads to a parametric modeling of the sulci [15]. First, a series of preprocessing aims at defining a region of interest (ROI) consisting of the union of gyri and sulci. Roughly, this ROI is obtained by first segmenting the brain and second by classifying the tissues into the three classes white matter, grey matter and cerebro-spinal fluid [14]. From this partition and in order to distinguish between sulci and gyri, it is resorted to differential geometry and particularly to the L_{vv} operator [8], which is a curvature extractor well adapted to a surface such as the cortex, since positive curvature characterizes the top of a gyrus, whereas negative curvature characterizes the bottom of a sulcus. This sulci/gyri partition results, after skeletonization, in the superficial topography of the cortex, that is to say in external traces of the sulci. Then, these external traces serve to initialize an active model extracting the surface of interest. The point is that the topology of the active model changes from 1D (active curve) to 2D (active surface). In fact, a set of potentials are defined such that the initial curve, located at the surface of the brain, evolves toward the bottom of the sulcus, thus initializing an active surface to optimize in order to extract the median surface of the sulcus. Finally, the choice of the parameterization has been fixed on a cubic B-spline surface, which is well adapted to model free form objects.

We thus dispose of a parametric representation of the shapes of interest through the B-spline modeling. The spline, parameterized by u and v, is described by nbp knots and $nbc = nbc\_u * nbc\_v$ control points where nbc_u (resp. nbc_v) is the number of control points in the direction associated with parameter u (resp. v). The parametric direction u represents the length of the sulcus and the direction v its depth. Giving nbc control points completely defines the sulcal surface. Consequently, we can represent a sulcus by the vector of its knots or its control points. The ratio nbc/nbp defines the smoothing factor: the smaller this ratio is, the smoother the surface will be (we have chosen $nbc/nbp = 1/24$). The main advantage to use control points is their compact but complete representation of each surface.

Since the statistical analysis used here needs to establish the point to point correspondences between all shapes of the training set, a registration and resampling stage is necessary.

Thus the sulci will be expressed in the same system of coordinates and will have the same number of points. It must be noted that the B-spline modeling makes it possible to change arbitrarily the parametrization without affecting the sulcus shape. Initially, each sulcus is expressed in the image coordinate system which is different from one subject to another. The idea is to associate its own system of coordinates with each sulcus, built so that it is common to all sulci. We call it "local coordinate system". It is useful to determine the rigid transformation (rotation+translation) aligning all local systems of axes and to apply it to the associated shapes.

Let $\mathcal{R}_s(O_s, \mathbf{u_s}, \mathbf{v_s}, \mathbf{w_s})$ be the local coordinate system of a sulcus. The origin O_s is the center of mass of the sulcus. Axes $\mathbf{u_s}$, $\mathbf{v_s}$ and $\mathbf{w_s}$ are defined as the axes of inertia of the sulcal surface, and are decided to be so that $\mathbf{u_s}$ follows the length of the sulcus, $\mathbf{v_s}$ its depth and $\mathbf{w_s}$ its normal. This discrimination between the three axes is first carried out by considering that $\mathbf{u_s}$ (resp. $\mathbf{v_s}$) is the axis of inertia the "most collinear" with the nbc_u (resp. nbc_v) pseudo-parallel directions; each of them being defined by the two extremities of a sulcus' line in direction u (resp. v). Then $\mathbf{w_s}$ is obtained by the vector product: $\mathbf{w_s} = (\mathbf{u_s} \wedge \mathbf{v_s})$.

The sulci have now to be expressed in their local coordinate systems. It amounts to determining, for each sulcus, the matrix $\mathbf{M}$ defining the change of basis from the local coordinate system $\mathcal{R}_s$ towards the image coordinate system, let it be $\mathcal{R}(O, \mathbf{u}, \mathbf{v}, \mathbf{w})$. Let $\mathbf{R}$ and $\mathbf{t}$ be the rotation matrix and the translation vector of the inverse change of basis $\mathbf{M^{-1}}$ (*i.e.* from $\mathcal{R}$ towards $\mathcal{R}_s$). Then in homogeneous coordinates:

$$\mathbf{M^{-1}} = \begin{pmatrix} \mathbf{R} & \mathbf{t} \\ 0\ 0\ 0 & 1 \end{pmatrix} \text{ where } \mathbf{R} = \begin{pmatrix} \mathbf{u_s} & \mathbf{v_s} & \mathbf{w_s} \end{pmatrix} \text{ and } \mathbf{t} = \overrightarrow{OO_s}$$

Since $\mathbf{R}$ is orthogonal:

$$\mathbf{M} = \begin{pmatrix} \mathbf{R}^T & -\mathbf{R}^T\mathbf{t} \\ 0\ 0\ 0 & 1 \end{pmatrix}$$

This transformation defines the local rigid registration process, which will be called LR in the following. Applying this rigid transformation to all the points of each sulcus aligns the training set as illustrated on Figure 1. Note that no homothety is performed in this LR method. As a matter of fact, the image data being acquired to the same scale, this enables to capture the inter-individual size variation in the shape model.

The next stage consists in resampling the sulci of the training set. We resample the elements of the training population on the one which has the most sample points, spline properties ensuring that the original shapes are preserved. Once the sulci are resampled and aligned, the matching is performed by just assigning control point to control point according to their curvilinear abscissa.

2.2 Statistical Analysis of Deformations

The statistical analysis of the training set leads to a modeling of cortical sulci and of their variations. The model captures the shape variability observed within the training set. As a matter of fact, the statistical analysis reveals the main modes of variation relative to a

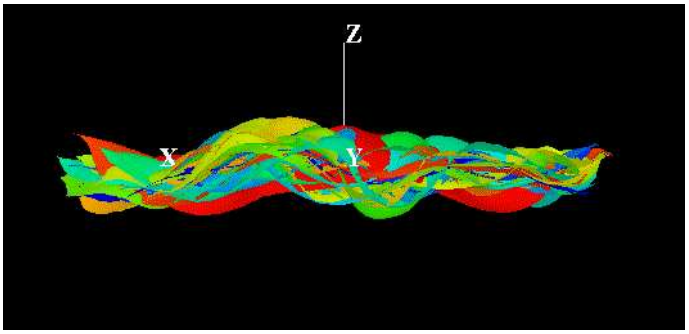

Figure 1: A side view of a database of 18 left central sulci aligned in the local coordinate system. The sulci come from a database made up of 18 healthy, right-handed, 35+/-10 years old males. Directions of the axes are for x axis: foot-head, for y axis: toward the outside of the brain, for z axis: antero-posterior.

reference shape, which can be the mean shape over the training set for instance. We use a principal component analysis which enables to represent data in a new basis, orthogonal, and which suppresses the redundancy of information. Moreover, this analysis enables a modal approximation, performed by retaining the most significant modes.

2.2.1 Principal Component Analysis.

Let $\mathcal{P}$ be the training population made up of N elements, $\mathbf{x}_i \in \mathcal{P}$ a shape, $\bar{\mathbf{x}}$ the mean shape on $\mathcal{P}$, $\mathbf{C}$ the covariance matrix. A shape $\mathbf{x}_{i,\, i=1\ldots N}$, is represented by the vector of control points of the spline that models the median surface of the sulcus:

$$\mathbf{x}_i = (x_{i_1}, y_{i_1}, z_{i_1}, \ldots, x_{i_n}, y_{i_n}, z_{i_n})^T \quad \text{with } n = nbc$$

The mean shape, used as the reference shape, and the covariance matrix are given by:

$$\begin{cases} \bar{\mathbf{x}} = \frac{1}{N} \sum_{i=1}^{N} \mathbf{x}_i \\ \mathbf{C} = \frac{1}{N} \sum_{i=1}^{N} d\mathbf{x}_i d\mathbf{x}_i^T \text{ with } d\mathbf{x}_i = \mathbf{x}_i - \bar{\mathbf{x}} \end{cases}$$

Diagonalizing the covariance matrix $\mathbf{C}$ provides the new modal basis Φ:

$$\mathbf{C} = \Phi \Lambda \Phi^T \text{ where } \Lambda = diag(\lambda_1, \ldots, \lambda_{3n}) \quad \text{with } \lambda_1 \geq \lambda_2 \geq \ldots \geq \lambda_{3n}$$

Then any shape $\mathbf{x}$ can be written: $\mathbf{x} = \bar{\mathbf{x}} + \Phi\mathbf{b}$ where $\mathbf{b} = (b_1, \ldots, b_{3n})^T$ is the vector of modal amplitudes of deformation and $(-\Phi\mathbf{b})$ corresponds to the deformation vectors in each point of $\mathbf{x}$ towards the mean shape. Since the eigenvalue λ_i is the variance explained by the i^{th} mode, a large part of the variability can be explained by retaining only the first m modes. The value m is chosen so that $\sum_{i=1}^{m} \lambda_i$, the variance explained by the first m modes,

represents a desired proportion, p, of the whole variance λ_T; that is to say m is such that $\frac{\sum_{i=1}^{m}\lambda_i}{\lambda_T} \simeq p$ where $\lambda_T = \sum_{i=1}^{3n}\lambda_i$. Retaining only m modes enables us to achieve a modal approximation:

$$\begin{cases} \mathbf{x} = \bar{\mathbf{x}} + \Phi_\mathbf{m}\mathbf{b_m} \\ \mathbf{b_m} = {\Phi_\mathbf{m}}^T(\mathbf{x} - \bar{\mathbf{x}}) \end{cases}$$

where $\Phi_\mathbf{m}$ is a submatrix of Φ containing the first m eigenvectors of $\mathbf{C}$, thus defining the modal approximation basis. The vector $\mathbf{b_m} = (b_1, \ldots, b_m)^T$ represents a shape in the m-dimensional space defined by the principal components. The analysis is convenient since this working space is of lower dimension (m). However, $\mathbf{b_m}$ must be constrained in order to represent an "allowable" shape (*i.e.* a shape consistent with the learnt shapes). Given the assumption that the distribution of vectors $\mathbf{x}_i$ is gaussian , the range of variability of each $b_{i,\, i=1\ldots m}$, is typically such as:

$$-3\sqrt{\lambda_i} \leq b_i \leq +3\sqrt{\lambda_i} \tag{1}$$

In fact, under the assumption $\mathbf{x}_i \sim \mathcal{N}(\bar{\mathbf{x}}, \mathbf{C})$, it comes that $b_i \sim \mathcal{N}(0, \lambda_i)$ and so $P(b_i \leq 3\sqrt{\lambda_i}) = 99.7\%$. Thus, (1) can be considered as a condition of representativity of the class of objects of interest.

2.2.2 Results.

Several tests have been carried out by making the cardinal of the training population vary (up to 85 sulci) and also by changing the type of sulci (central sulcus, lateral sulcus, superior frontal sulcus, ... of both hemispheres). We present the results obtained on a training set made up of the 18 left central sulci registered in the previous stage. These sulci come from a database consisted of 18 volunteers, all males, 35+/-10 years old, healthy and right-handed, who underwent a T1-MR SPGR 3D study. Figure 3 shows the predominance of the first modes. Indeed, the first 5 modes explain a large part of the total variation (about 70%). The first mode explains on its own almost 30% of the total variation (whereas a sulcus is described by 104 control points, that is to say 312 variables, and by more than 8000 variables if knots are considered). Figure 4a shows the variations around the mean shape (Fig. 2) due to the first mode. They are mainly relative to the length and to the torsion of the sulcus. On the contrary, Figure 4b illustrates the minor influence of the 15^{th} mode: the deformations are hardly distinct, all the sulci are almost superimposed to the mean shape. Accordingly this statistical modeling is appropriate to express the shapes and the variations in a compact and meaningful way.

3 Deformation Fields and Non-linear Registration

The deformation field ($-\Phi_\mathbf{m}\mathbf{b_m}$) obtained between a given sulcus and the mean sulcus can be extended to the vicinity of the considered sulcus by using an appropriate interpolation, the thin-plate spline interpolation in our case [6], [1], [20]. It can then be applied to any

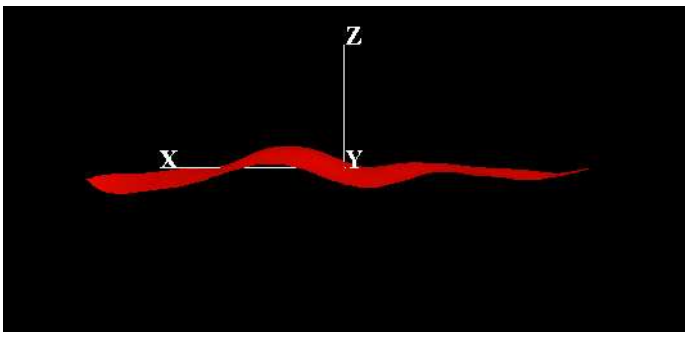

Figure 2: A side view of the mean left central sulcus of the training set consisted of the 18 left central sulci.

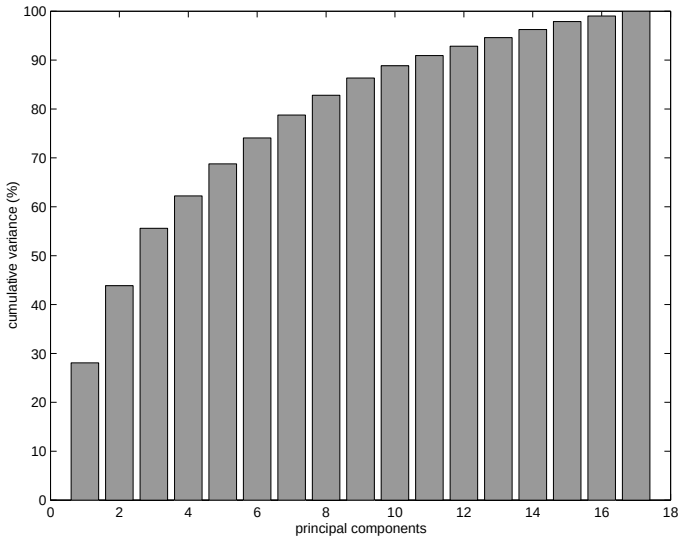

Figure 3: Cumulative variance according to the number of principal components retained. The training set consists of 18 left central sulci.

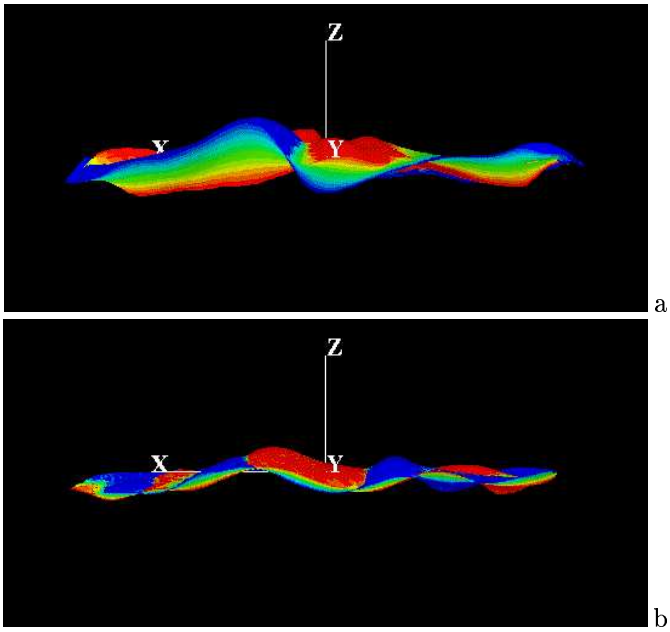

Figure 4: a) variations of the first mode around the mean sulcus, $-3\sqrt{\lambda_1} \leq b_1 \leq +3\sqrt{\lambda_1}$. b) variations of the 15^{th} mode around the mean sulcus,$-3\sqrt{\lambda_{15}} \leq b_{15} \leq +3\sqrt{\lambda_{15}}$.

object associated with this sulcus. We take advantage of this extension of the deformation field ($-\mathbf{\Phi_m b_m}$) to register sparse functional data (MEG dipoles in our case) located in the left central sulcus area towards a referential relative to the mean left central sulcus.

3.1 Interpolation using the Thin-Plate Spline Method

The use of thin-plate spline interpolation for registration purpose in medical imaging was first proposed by Bookstein. In [1], he proposes an algebraic approach to describe deformations specified by two sets of corresponding points. This method provides an interpolation function f which maps one of the two sets of corresponding points, the source set, onto the other one, the target set. Moreover, the function f is defined in some neighborhood of the set of source points so that it can be applied to a point in the source space to find its homologous in the target space.

Let $\mathcal{P} = \{P_i(x_i, y_i, z_i), i = 1, \ldots, n\}$ be the set of source points in the Euclidean space, and $\mathcal{V} = \{V_i = (x'_i, y'_i, z'_i), i = 1, \ldots, n\}$ the set of target points. The set $\mathcal{P}$ describes a shape $\mathbf{x}$, expressed by $\bar{\mathbf{x}} + \mathbf{\Phi_m b_m}$ according to our model. Let $r_{ij} = |P_i - P_j|$ be the Euclidean distance between two source points P_i and P_j. Then the function f is the sum of two terms: an affine part which represents its behavior at infinity, and a second part which is

asymptotically flat:

$$f(x,y,z) = a_1 + a_x x + a_y y + a_z z + \sum_{j=1}^{n} w_j U(|P_j - (x,y,z)|) \tag{2}$$

where

- the basis function U is the fundamental solution of the biharmonic equation $\Delta^2 U = \delta(0,0)$, δ being the Kronecker's function. It can be shown [2] that the equation of a thin uniform metal plate originally flat and now bent by vertical displacements is directly related to the biharmonic equation. In 3D the function U is $U(r) = |r|$ (whereas $U(r) = r^2 \ln r$ in 2D and $U(r) = |r|^3$ in 1D);

- the coefficients $\mathbf{a} = (a_1, a_x, a_y, a_z)^T$ and $\mathbf{w} = (w_1, w_2, \ldots, w_n)^T$ are obtained by solving the linear system:

$$\begin{cases} \mathbf{Kw} + \mathbf{Pa} = \mathbf{v} \\ \mathbf{P}^T\mathbf{w} = 0 \end{cases} \qquad \text{where} \quad \mathbf{P} = \begin{pmatrix} 1 & x_1 & y_1 & z_1 \\ \vdots & \vdots & \vdots & \vdots \\ 1 & x_n & y_n & z_n \end{pmatrix} ,$$

  $\mathbf{K}$ is a $n \times n$ matrix, whose general term is $(U(r_{ij}))_{1 \le i,j \le n}$, and $\mathbf{v}$ is the vector of one coordinate of the target set (*e.g.* $\mathbf{v} = (x'_1, \ldots, x'_n)$, what implies that (2) must be expressed for $f_x(x,y,z)$, $f_y(x,y,z)$ and $f_z(x,y,z)$).

Regarding the target set as the mean shape $\bar{\mathbf{x}}$, the deformation field $(-\Phi_\mathbf{m}\mathbf{b}_\mathbf{m})$ is then represented by the elements of $(\mathbf{w} \mid \mathbf{a})$, and it is extended outside the source shape $\mathbf{x}$ thanks to the function f.

3.2 Remark

The function f is defined on $\mathbb{R}^3$, but has to be applied only in the vicinity of the constraint. As a matter of fact, we are interested in propagating the deformation all over the "influence range" of the sulcus of interest, but not all over the brain. Therefore it is desirable to explicitly limit the influence of the thin-plate spline interpolation to a pre-defined neighborhood of the concerned sulcus. This can be achieved by defining a parallelepipedic bounding volume, V, specifying the neighborhood. However, in order to preserve the continuity of the transformation, we define a "fuzzy volume" through which the deformation will cancel itself out in a continuous way. This fuzzy volume can be described through a function, μ_V, defined as:

$$\begin{array}{rccc} \mu_V : & \mathbb{R}^3 & \longrightarrow & \mathbb{R} \\ & X = (x,y,z) & \longmapsto & \mu_{V_x}(x).\mu_{V_y}(y).\mu_{V_z}(z) \end{array}$$

where functions $\mu_{V_\cdot}$ have the following properties:

- defined on $\mathbb{R}$,
- C^2, *i.e.* twice differentiable and the second order derivative is continuous,
- decreasing on $\mathbb{R}^+$,
- even (this last property is sufficient when working in the local space),
- $\exists t \in \mathbb{R}^{+*}$ such that $\mu''_{V_.}(t) = 0$, $\mu''_{V_.}$ being the second order derivative of $\mu_{V_.}$;

where V_x, V_y and V_z specify the limits of the bounding box in x, y and z direction. For example, if $V_x = [-t_x, t_x]$ then μ_{V_x} will be chosen such that $\mu''_{V_x}(t_x) = 0$

Given such a μ_V function, let a point $X = (x, y, z) \in \mathbb{R}^3$ and $X_f = (x_f, y_f, z_f)$ be its image point by the thin-plate spline interpolation limited to one neighborhood V. Then,

$$X_f = f(X).\mu_V(X) + X.\mu_{\bar{V}}(X)$$

where $\mu_{\bar{V}} = 1 - \mu_V$.

The choice of μ_V as well as the tune of the limits of the box is incumbent upon an expert, and will play a role if deformation fields from different sulci are desired to be used, or if data out of the vicinity of the sulcus have to be treated for example. However, a single rule could be for instance to define t_z as the "mid-thickness" of a gyrus, where the mid-thickness of a gyrus could be half the distance between the gravity centers of its two bounding sulci (like central and postcentral sulci for the postcentral gyrus for example). Figure 5 gives examples of possible functions $\mu_{V_.}$:

1. $\forall t \in \mathbb{R}$, $\mu^{(1)}_{V_.}(t) = \frac{1}{1+kt^2}$, $k > 0$
2. $\forall t \in \mathbb{R}, \mu^{(2)}_{V_.} = \begin{cases} 1 & \text{if } 0 \leq |t| \leq a \\ \frac{1}{2} - \frac{1}{2} sin[\frac{\Pi}{b-a}(|t| - \frac{a+b}{2})] & \text{if } a \leq |t| \leq b \\ 0 & \text{if } b \leq |t| \end{cases}$
   with a and $b \in \mathbb{R}^+$ such that $a < b$
3. $\forall t \in \mathbb{R}$, $\mu^{(3)}_{V_.}(t) = e^{-kt^2}$, $k > 0$

We have simulated a set of source and target points (see Fig. 6, top), and computed the f function corresponding to these two sets. Figure 6, bottom, shows the result of the application of f on the whole grid. Although the deformation weakens far from the constraint, it remains influent. Conversely Fig. 7 illustrates the effect of the application of a restriction of f to a specified neighborhood; Fig. 7 top, via a door function, Fig. 7 bottom, via one μ_V function. The limitation of the deformation via a door function is efficient, but does not preserve the continuity. On the other hand, the restriction of the extrapolation to the vicinity of the constraint via one μ_V function is effective and continuity preserving, as can be seen on Fig. 7, bottom.

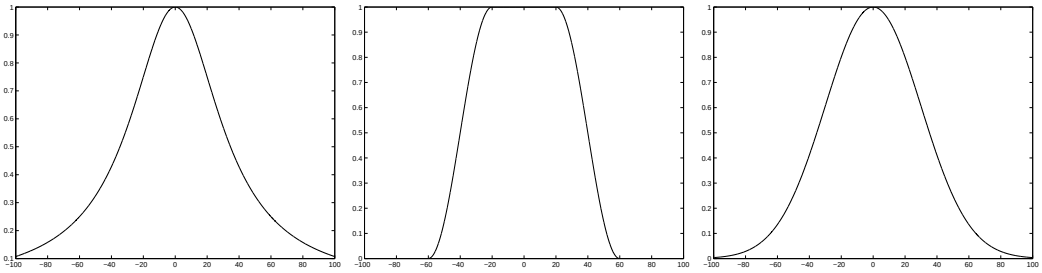

Figure 5: Examples of $\mu_{V_.}$ functions. From left to right: $\mu_{V_.}^{(1)}$ (inverse) such that $\mu_{V_.}^{(1)\,''}(20) = 0$; $\mu_{V_.}^{(2)}$ (sinus) such that $\mu_{V_.}^{(2)\,''}(40) = 0$; $\mu_{V_.}^{(3)}$ (exponential) such that $\mu_{V_.}^{(3)\,''}(30) = 0$.

3.3 Results

The statistical modeling of anatomical structures such as cortical sulci, combined with a consistent extrapolation of deformations, can now be used to register functional activations in a non-linear and local way by using the method described above. In a first part, we detail the results obtained with the method described previously (NLL). We present two tests differing by the number of modes, m, used in the construction of the deformation field $(-\mathbf{\Phi_m b_m})$. The first one is performed with all the modes ($m = 17$) whereas the second one is performed with only five modes ($m = 5$). The NLL method applied in the first (resp. second) case is called NLL1 (resp. NLL2). In a second part, we compare the NLL approach with three inter-individual global registration methods. These methods have in common to seek a global transformation between the source volume and the target volume, the target being one subject of the database chosen as a reference. They differ in their similarity measure and their type of transformation. They are:

- a global rigid method (GR): registration due to the maximization of mutual information [3], [26];
- a global piecewise affine registration (PS): the Talairach Proportional Squaring [24]. An affine transformation is comptuted on each of the 12 sub-volumes defined by the Talairach Proportional Squaring;
- a non-linear global registration (NLG): a method based on optical flow and on a robust optimization scheme to estimate a dense vector field [12]. This dense deformation field is computed at a resolution grid in the order of $1mm$.

For comparison purpose, results for local methods as well as for global methods will be expressed in the local coordinate system. The local registration performed with the transformation described by the matrix $\mathbf{M}$ (see Sect. 2.1), has then to be applied to the results of each method. This local registration, called local rigid method (LR), is therefore a sort of constant in all methods and will so serve as a reference. Accordingly, the comparison part

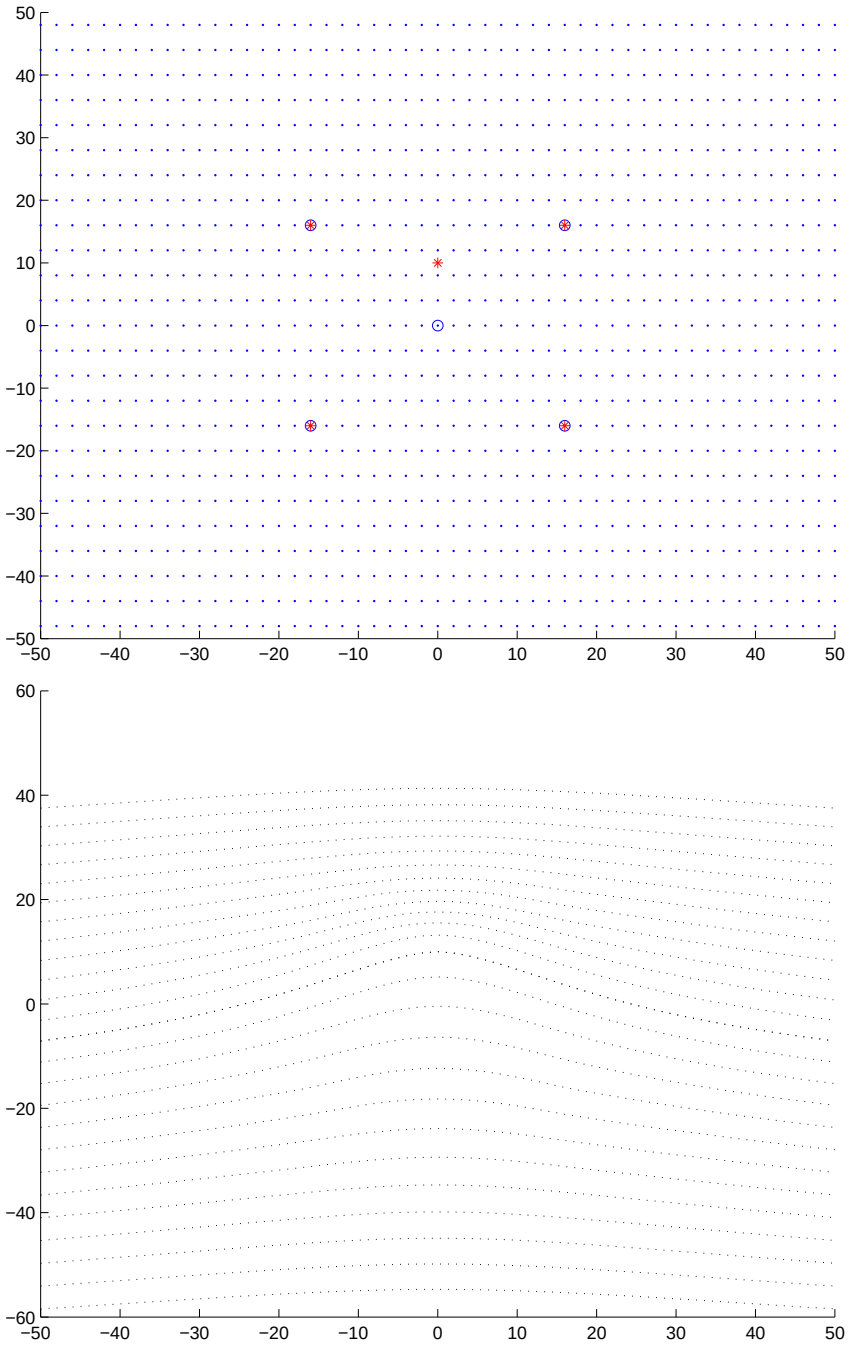

Figure 6: Top: simulated data: blue circles are source points, red asterisks are target points, blue points are the initial grid. Bottom: The initial grid is deformed by applying the f function computed from the sets of source and target points.

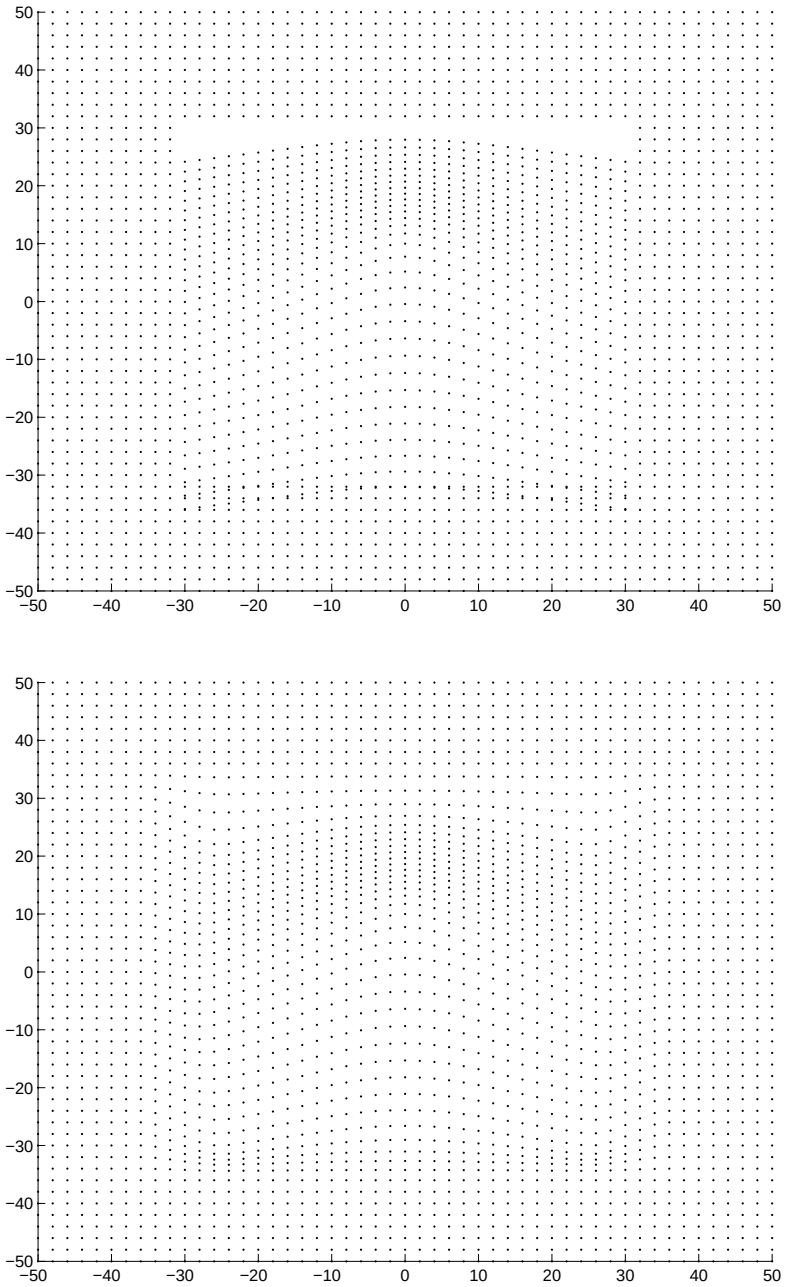

Figure 7: The application of the f function is restricted thanks to: top, a non-continuous function (a door function); bottom, a continuous function (the sinus function presented in Section 3).

deals with 6 methods: 3 local methods (LR, NLL1, NLL2) and 3 global methods (GR, PS and NLG).

For all methods, the functional data to register are MEG dipoles corresponding to a somatosensory activation of right hand fingers (thumb, index, little finger) performed for 15 volunteers out of the 18 subjects of our database. We recall that the database is made up of $35 + / - 10$ years old healthy males, all right-handed having also underwent a T1-MR SPGR 3D study (see Sect. 2). MEG current dipoles have been reconstructed using a spatiotemporal algorithm [21], and selected by choosing the most significant one in the 45+/-15 ms window. Thus, three dipoles, one per finger, are available for each of the 15 volunteers. The somatosensory paradigm chosen here is a very simple well-known one and is thus convenient to test our approach, since our objective is not to explain complex physiological processes but rather to study the behavior of such a registration method. Thus the considered dipoles are expected to follow a somatotopic organization. First, they must be located in the left central sulcus area, and more precisely in the back of the central sulcus, *i.e.* in the post-central gyrus. Second, they must be identically ordered on the gyrus through the database, *i.e.* from the little finger to the thumb via the index according to the head-foot direction. Despite the simplicity of the protocol, reconstruction of the sources in MEG [21], and MEG/MRI registration [22], remain challenging tasks and the positions of the MEG dipoles can be marred with errors. As a consequence, some of the dipoles are obviously mislocalized, like those situated at the wrong side of the sulcus for example.

3.3.1 Method NLL.

We apply the thin-plate spline method to merge anatomical and functional information in the coordinate system of the mean central sulcus. First, we rigidly register each dipole towards the local space by applying the transformation described by the corresponding matrix $\mathbf{M}$ (see Sect. 2), *i.e.* by using the LR method (see Fig. 8a). Then, for each subject, we compute the "field" $(\mathbf{w} \mid \mathbf{a})$ between the left central sulcus of this subject and the mean sulcus. We apply it to the three dipoles of this subject, the field $(-\mathbf{\Phi_m b_m})$ being computed with all the modes ($m = 17$, method NLL1). Figure 8b shows that dipoles gather around the plane of the mean sulcus.

To numerically quantify this observation, we compute the dipole localization covariance matrix and its determinant, what provides objective measures of the 3D dispersion of the registered dipoles. The determinant (see Table 1, local methods) indicates a smaller dispersion for method NLL1. Similarly, as it can be seen in Table 2 (local methods), the standard deviation (we exhibit standard deviation along each axis rather than covariance to have same size unit as a sulcus, *i.e.* *mm*) along axes x, y and particularly z is considerably reduced. The flattening in the z direction can be expected since the deformation is normal to mean sulcus plane in this referential. Furthermore, as shown in Fig. 9, the resulting dipoles are correctly located with respect to the concerned finger: the somatotopic organization is preserved.

We present a second test in which we consider only 5 modes in the construction of $(-\mathbf{\Phi_m b_m})$, and call this method NLL2. This approximation smoothes the sulcus and dis-

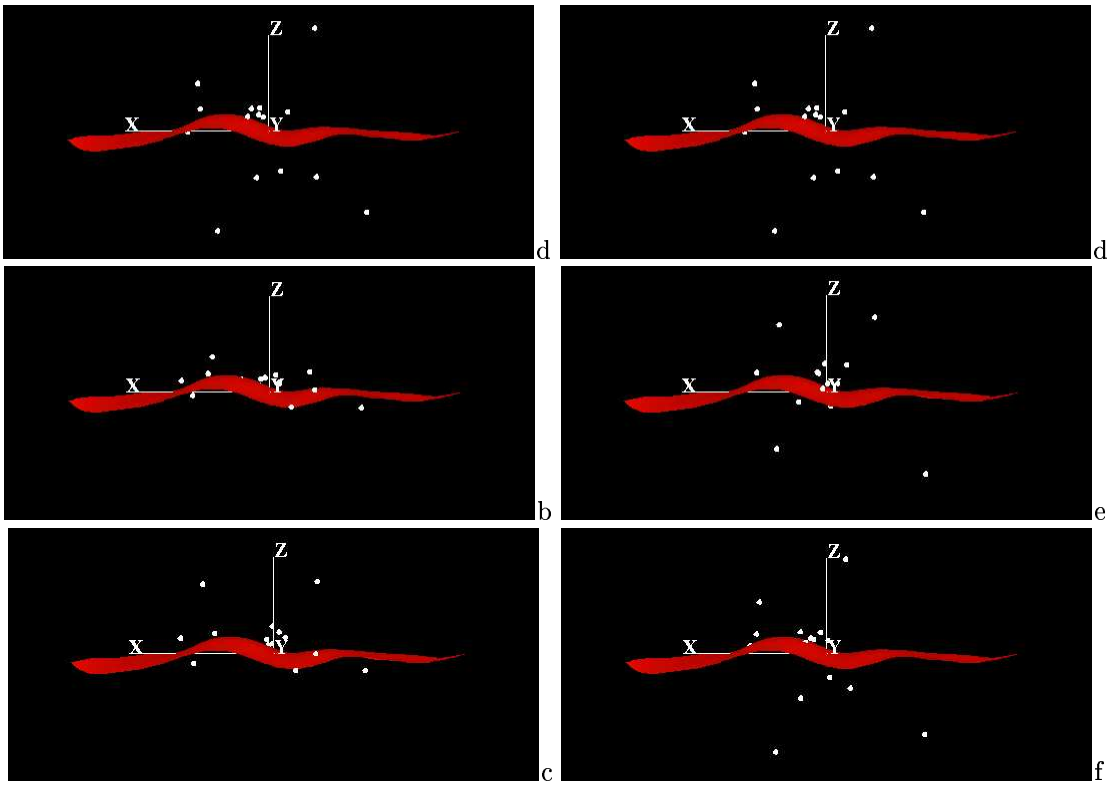

Figure 8: Registration of MEG dipoles (somatosensory activation of the thumb): the sulcus is the mean left central sulcus. a) method LR: the dipoles are rigidly registered. b), c) method NLL: the dipoles are registered via the deformation field , b) $m = 17$, c) $m = 5$. d) method GR. e) method PS. f) method NLG.

Local Methods	LR	NLL1 (m=17)	NLL2 (m=5)
thumb	217671	6439	30793
index finger	292114	13479	45125
little finger	343260	18735	91921
Global Methods	GR	PS	NLG
thumb	175873	65201	119487
index finger	241181	112660	245742
little finger	268867	98649	270147

Table 1: The determinant of the covariance matrix of MEG dipoles localizations for somatosensory activations (thumb, index, little finger) after local registration methods: local rigid registration (LR), thin-plate spline interpolation based registration (NLL1 for m=17 and NLL2 for m=5), and after global registration methods (GR, PS and NLG).

Local Methods	LR			NLL1 ($m = 17$)			NLL2 ($m = 5$)		
thumb	10.33	5.78	9.77	9.90	5.26	2.66	10.15	5.22	5.19
index finger	10.07	6.11	9.40	9.44	5.98	2.38	9.77	5.73	4.06
little finger	10.32	6.67	10.28	9.73	6.35	2.81	9.94	6.39	5.56
Global Methods	GR			PS			NLG		
thumb	9.85	4.71	10.45	8.84	3.88	7.96	8.91	4.77	9.90
index finger	9.86	5.38	9.78	9.17	5.15	7.96	9.26	6.19	9.13
little finger	10.04	5.55	10.37	9.36	4.91	7.25	9.61	6.16	9.84

Table 2: The standard deviation along x, y and z of MEG dipoles localizations for somatosensory activations (thumb, index, little finger) after local rigid registration (LR), thin-plate splines interpolation based registration (NLL) for $m = 17$ and $m = 5$, and global registration (methods GR, PS, NLG). The figures have mm unit, knowing that 100, 30, 23 mm are an order for the length (x axis), the depth (y axis), the thickness (z axis) dimensions of a sulcus.

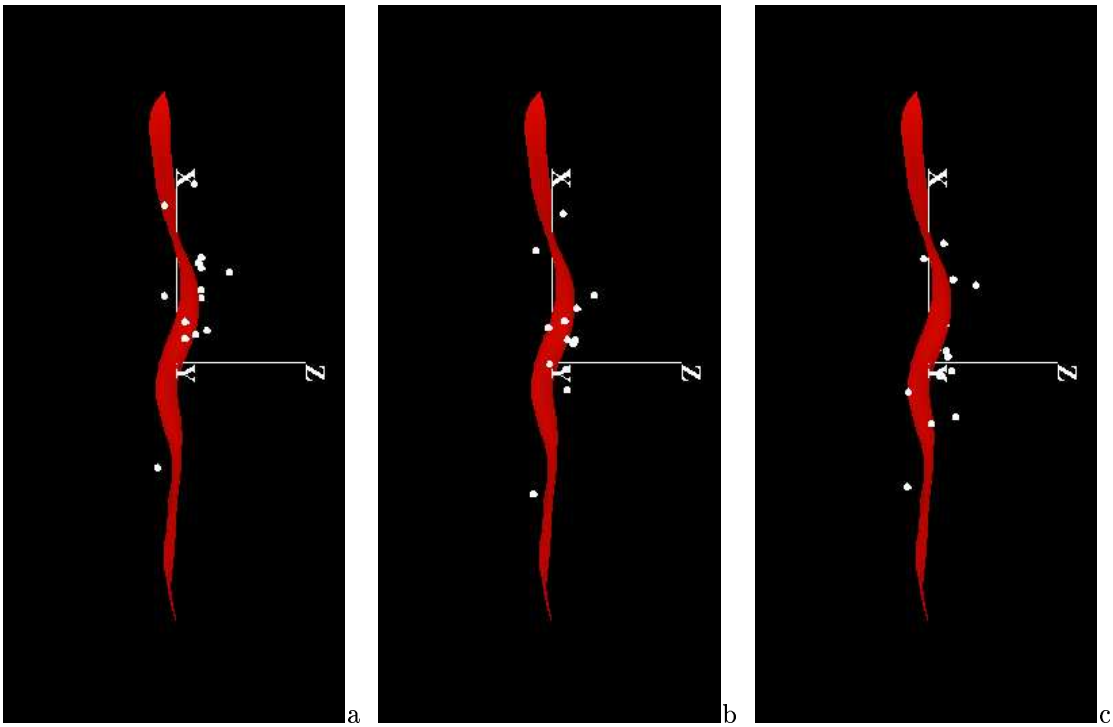

Figure 9: Illustration of the somatotopy of the registered dipoles (method NLL1). The dipoles corresponding to each finger are ordered. a) the registered dipoles corresponding to the little finger. b) the registered dipoles corresponding to the index. c) the registered dipoles corresponding to the thumb.

cards minor modes possibly resulting from potential segmentation errors of initial data. Results are presented in Figure 8c, Table 1 (local methods) and Table 2 (local methods). With a limited number of modes (5), we observe that dispersion of the dipoles, in accordance with the determinant of the covariance matrix, is larger than with all the modes (17), but still lower than with LR method.

The assumption underlying this study, stating that a part of the functional inter-subject variability is encoded in the anatomical variability, also states that a part is decorrelated from the anatomy and cannot be reduced with an anatomical matching. The results show that the initial functional inter-subject variability is indeed reduced, and that the residual variability we can observe results from this irreducible variability plus, of course, the errors coming from the preprocessing stages (multimodal registration, dipoles reconstruction, ...).

3.3.2 Comparison.

We apply each of the three global inter-individual registration methods GR, PS and NLG, to MEG data. For comparison purpose, we place the resulting dipoles in the local space via the LR method, and also visualize them superimposed to the mean sulcus. Figure 8 shows that method NLL gives the best results in terms of dipoles gathering while global methods seem to lead to similar dispersion.

As mentioned previously, it is possible to numerically assess these visual results by computing objective measures of the 3D dispersion of the registered dipoles, that is to say the dipole localization covariance matrix (see Table 2), as well as its determinant (see Table 1). These measures show a decrease of variance for NLL methods mainly in z direction, whereas global methods, linear or not, keep quite similar dispersions. However we note a weaker dispersion for method PS than for GR and NLG methods.

These results are confirmed by performing some statistical hypothesis tests. Such tests usually assume one hypothesis, say H_0, against another one, say H_1, which can be as simply as $\neg H_0$. One has to fix beforehand a probability α which is the probability to choose H_1 whereas H_0 is true (typical values for α are 0.01, 0.05, 0.1). In other words, if H_0 has only a probability α to occur, then it is rejected and H_1 is accepted.

The tests we use in the following are the ANOVA (ANalysis Of VAriance) test and the Fisher-Snedecor and Student test. ANOVA is used to determine if significant differences exist among several populations. It tests the equality of the sample means by using a criterion based on the inter and intra variance samples, samples assumed to be gaussian. The Fisher-Snedecor and Student test is supposed to determine if two samples, assumed to be independent, come from a same population with respect to a studied variable, by testing first the equality of their variances (Fisher-Snedecor test) and second the equality of their mean in case variances are said to be the same (Student test). These tests set "H_0: variances (or means) are equal" and "H_1: variances (or means) are not equal". Note that the Fisher-Snedecor test also assumes the gaussianity of the law of the studied variable through the samplings, whereas the Student test is robust to a change of law.

In the following, we consider a group of dipoles, corresponding to one given finger, and registered by one registration method, as a sample. Then, for one given finger, the applica-

	skewness min/max	kurtosis min/max		skewness min/max	kurtosis min/max
x_{thumb}	0.0005/0.8425	2.4574/4.0438	$\sqrt{(x-\bar{x})^2}_{thumb}$	0.4839/1.3504	2.0740/4.5226
x_{index}	0.4810/1.4287	3.9669/5.6016	$\sqrt{(x-\bar{x})^2}_{index}$	1.4147/2.1091	3.9860/7.0360
x_{little}	0.6562/1.3324	4.0228/5.2678	$\sqrt{(x-\bar{x})^2}_{little}$	1.6381/2.3251	4.9314/8.1926

	skewness min/max	kurtosis min/max		skewness min/max	kurtosis min/max
y_{thumb}	0.0472/0.4998	2.5381/4.1085	$\sqrt{(y-\bar{y})^2}_{thumb}$	0.8875/1.3058	3.0890/4.0720
y_{index}	0.2306/1.3830	2.4593/4.6833	$\sqrt{(y-\bar{y})^2}_{index}$	0.6091/1.6985	1.9480/5.7243
y_{little}	0.1656/0.7838	2.0850/4.6484	$\sqrt{(y-\bar{y})^2}_{little}$	0.4626/1.7176	2.1282/3.7000

	skewness min/max	kurtosis min/max		skewness min/max	kurtosis min/max
z_{thumb}	0.1590/0.9797	2.8163/3.5032	$\sqrt{(z-\bar{z})^2}_{thumb}$	0.9703/1.0828	2.5242/2.9134
z_{index}	0.1609/0.8746	2.3398/3.3845	$\sqrt{(z-\bar{z})^2}_{index}$	0.5540/1.1534	1.9566/3.8071
z_{little}	0.0595/0.8832	2.4401/2.8307	$\sqrt{(z-\bar{z})^2}_{little}$	0.5758/0.9970	2.1236/2.7691

Table 3: Minimum and maximum over the 6 considered samples for each finger of the skewness and kurtosis with respect to the following variables: x, y, z and $\sqrt{(x-\bar{x})^2}$, $\sqrt{(y-\bar{y})^2}$, $\sqrt{(z-\bar{z})^2}$. A gaussian distribution has skewness equal to 0 and kurtosis equal to 3. For a sample size equal to 15, empirical skewness must be inferior to the critical value v_s, which is $v_s = 0.851$ at $\alpha = 0.05$ and $v_s = 1.272$ at $\alpha = 0.1$; empirical kurtosis must be between 1.72 and 4.13 at $\alpha = 0.05$.

tion of each of the 6 tested registration methods produces 6 samples and the independence assumption between samples can be admitted. Note that, for one given finger, ANOVA considers all the 6 samples at once whereas Fisher-Snedecor and Student tests use them two-by-two. That means tests must be repeated for each of the three fingers, and in case of Fisher-Snedecor and Student tests, for each possible couple of methods. Thus performing theses tests enables to compare the methods globally in case of ANOVA, or by pairs in case of Fisher-Snedecor and Student tests, and to conclude if they produce results significantly different in a statistical sense.

We have first chosen to examine the dipole localization through the separated study of the coordinates x, y and z. The computation of the skewness and kurtosis of the variables x and y reveal a certain non-gaussianity of these distributions (see Table 3), except for the thumb finger. So we have performed a Fisher-Snedecor test only on the x and y distributions of the thumb finger, let them be x_{thumb} and y_{thumb}. It shows no significant difference between the methods with $\alpha = 0.05$. However we note a difference between LR and PS for the y_{thumb} distribution with $\alpha = 0.1$. A Student test performed, still on x and y distributions, but this time for each of the three fingers (*i.e.* on x_{thumb}, x_{index}, x_{little}, y_{thumb}, y_{index} and y_{little})

$\sqrt{(z-\bar{z})^2}_{thumb}$	3.4187
$\sqrt{(z-\bar{z})^2}_{index}$	3.9122
$\sqrt{(z-\bar{z})^2}_{little}$	3.6766

Table 4: Values F^* from the ANOVA for tests performed on the 6 samples corresponding to the 6 registration methods (LR, NLL1, NLL2, GR, PS, NLG) for each of the three fingers with respect to the variable $\sqrt{(z-\bar{z})^2}$. Methods are concluded to be significantly different if $F^* > F$ with $F = 2.33$ at $\alpha = 0.05$.

reveals some difference between PS and methods NLL1, NLL2 and NLG, but only for the y distribution. More precisely, it appears between PS and NLL1 for y_{thumb} with $\alpha = 0.05$, and for y_{little} with $\alpha = 0.1$; and between PS and methods NLL2 and NLG for y_{thumb} with $\alpha = 0.1$. As far as the z coordinate is concerned, since the computation of the skewness and kurtosis does not reject the gaussian assumption (see Table 3), we have performed a Fisher-Snedecor test for each of the three fingers (*i.e.* on z_{thumb}, z_{index} and z_{little}). It concludes for a significant difference between NLL methods and all the others with $\alpha = 0.05$, except between NLL2 and PS for which difference is less obvious: a difference appears only for index with $\alpha = 0.05$ and for thumb with $\alpha = 0.1$. We note a difference between PS and GR methods for little finger with $\alpha = 0.1$.

Another way to examine the dispersion of the dipoles is to study the distribution of the distance, along each axis, between a dipole and its mean dipole, that is to say to study the variables $\sqrt{(x-\bar{x})^2}$, $\sqrt{(y-\bar{y})^2}$, and $\sqrt{(z-\bar{z})^2}$. Since the distributions of $\sqrt{(x-\bar{x})^2}$ and $\sqrt{(y-\bar{y})^2}$ are very unlikely gaussian (see Table 3), we have applied to them a Student test[1]. It does not show any difference between methods with respect to these variables. On the contrary, an ANOVA test achieved on the samplings defined by the variable $\sqrt{(z-\bar{z})^2}$ [2] (whose law are not said to be ungaussian according to their skewness and kurtosis, see Table 3) shows the existence of a statistical difference between the methods with $\alpha = 0.05$, as it can been seen on Table 4. More precisely, when performing a Fisher-Snedecor test on these same samplings, a significant difference appears between NLL and other methods with $\alpha = 0.05$ (once again except between NLL2 and PS for thumb where a difference appears only with $\alpha = 0.1$, and for little finger where no difference appears). We also note a difference between PS and methods LR, GR and NLG for little finger with $\alpha = 0.1$. One can find all figures concerning the performed Fisher-Snedecor tests in Table 5, and those concerning the performed Student tests in Tables 6 and 7.

We state a significant difference between local and global methods. The case of the PS method, which distinguishes itself from the other global methods, may be explained since method PS is by construction relevant and precise in the central region (it in fact relies

[1] Still studying the samples corresponding to each of the three fingers in a separate way, the tested variables are in this case $\sqrt{(x-\bar{x})^2}_{thumb}$, $\sqrt{(x-\bar{x})^2}_{index}$, $\sqrt{(x-\bar{x})^2}_{little}$, $\sqrt{(y-\bar{y})^2}_{thumb}$, $\sqrt{(y-\bar{y})^2}_{index}$ and $\sqrt{(y-\bar{y})^2}_{little}$.

[2] Similarly, the tested variables are in this case $\sqrt{(z-\bar{z})^2}_{thumb}$, $\sqrt{(z-\bar{z})^2}_{index}$ and $\sqrt{(z-\bar{z})^2}_{little}$.

	x_{thumb}	y_{thumb}	z_{thumb}	z_{index}	z_{little}	$\sqrt{(z-\bar{z})^2}_{thumb}$	$\sqrt{(z-\bar{z})^2}_{index}$	$\sqrt{(z-\bar{z})^2}_{little}$
LR/NLL1	1.089	1.207	**13.442**	**15.529**	**13.420**	**12.026**	**12.148**	**12.935**
LR/NLL2	1.035	1.226	**3.544**	**5.352**	**3.416**	**2.727**	**4.059**	**2.727**
LR/GR	1.098	1.507	1.143	1.083	1.018	1.010	1.410	1.017
LR/PS	1.365	*2.220*	1.508	1.394	2.007	1.166	1.139	*2.195*
LR/NLG	1.345	1.469	1.026	1.061	1.091	1.008	1.248	1.052
NLL1/NLL2	1.052	1.016	**3.793**	**2.902**	**3.928**	**4.410**	**2.993**	**4.742**
NLL1/GR	1.089	1.249	**15.369**	**16.815**	**13.661**	**12.145**	**17.130**	**13.160**
NLL1/PS	1.253	1.840	**8.912**	**11.141**	**6.685**	**10.314**	**10.666**	**5.893**
NLL1/NLG	1.235	1.217	**13.794**	**14.641**	**12.301**	**11.930**	**15.162**	**12.296**
NLL2/GR	1.061	1.229	**4.052**	**5.795**	**3.477**	**2.754**	**5.723**	**2.775**
NLL2/PS	1.318	1.811	*2.349*	**3.840**	1.702	*2.339*	**3.563**	1.243
NLL2/NLG	1.299	1.198	**3.637**	**5.046**	**3.131**	**2.705**	**5.066**	**2.593**
GR/PS	1.242	1.473	1.725	1.509	*2.043*	1.177	1.606	*2.233*
GR/NLG	1.224	1.026	1.114	1.148	1.110	1.018	1.130	1.070
PS/NLG	1.015	1.511	1.548	1.314	1.840	1.157	1.421	*2.086*

Table 5: Values of the Fisher-Snedecor variable, F^*, for tests performed on each pair of registration methods (LR, NLL1, NLL2, GR, PS and NLG) with respect to the variables: x and y (for thumb samples), z and $\sqrt{(z-\bar{z})^2}$ (for thumb, index and little finger samples) . Given two samples of size n and having empirical variances σ_1^2 and σ_2^2 then $F^* = F^*_{n-1} = \frac{\sigma_1^2}{\sigma_2^2}$; and these two samples are significantly different if $F^* > F_{14}$ with $F_{14} = 2.48$ at $\alpha = 0.05$ and $F_{14} = 2.02$ at $\alpha = 0.1$. In bold (*resp.* in italics) figures indicate a significant difference at $\alpha = 0.05$ (*resp.* $\alpha = 0.1$).

	x_{thumb}	x_{index}	x_{little}	y_{thumb}	y_{index}	y_{little}
LR/NLL1	0.0976	0.1137	0.0865	0.6634	0.5290	0.4257
LR/NLL2	0.0266	0.0129	0.0453	0.4177	0.3496	0.2397
LR/GR	0.0542	0.0676	0.0563	0.6496	0.4801	0.6421
LR/PS	0.1337	0.1963	0.2791	1.4421	1.0336	1.2120
LR/NLG	0.3437	0.3101	0.2219	0.0852	0.0745	0.0354
NLL1/NLL2	0.0713	0.1288	0.1349	0.2607	0.1922	0.1894
NLL1/GR	0.0445	0.0451	0.0298	1.4203	1.0489	1.1264
NLL1/PS	0.0317	0.0839	0.1972	**2.3289**	1.6213	*1.7404*
NLL1/NLG	0.4569	0.4394	0.3185	0.6403	0.4536	0.4069
NLL2/GR	0.0275	0.0816	0.1033	1.1517	0.8702	0.9203
NLL2/PS	0.1064	0.2130	0.3324	*2.0439*	1.4529	1.5212
NLL2/NLG	0.3756	0.3017	0.1794	0.3698	0.2728	0.2133
GR/PS	0.0788	0.1278	0.2243	0.8518	0.5843	0.6035
GR/NLG	0.4112	0.3839	0.2835	0.8118	0.5591	0.7111
PS/NLG	0.5183	0.5305	0.5231	*1.7369*	1.1141	1.3158

Table 6: Values of the Student variable, T^*, for tests performed on each pair of registration methods (LR, NLL1, NLL2, GR, PS and NLG) with respect to the variables: x and y (for thumb, index and little finger samples). Given two samples of size n and having empirical means $\bar{x}_1$ and $\bar{x}_2$, and empirical variances σ_1^2 and σ_2^2, then $T^* = T^*_{2(n-1)} = \frac{\bar{x}_1 - \bar{x}_2}{\sqrt{(\sigma_1^2+\sigma_2^2)}}\sqrt{(n-1)}$; and these two samples are significantly different if $T*{>}T_{28}$ with $T_{28} = 2.048$ at $\alpha = 0.05$ and $T_{28} = 1.701$ at $\alpha = 0.1$. In bold (*resp.* in italics) figures indicate a significant difference at $\alpha = 0.05$ (*resp.* $\alpha = 0.1$).

	$\sqrt{(x-\bar{x})^2}_{thumb}$	$\sqrt{(x-\bar{x})^2}_{index}$	$\sqrt{(x-\bar{x})^2}_{little}$	$\sqrt{(y-\bar{y})^2}_{thumb}$	$\sqrt{(y-\bar{y})^2}_{index}$	$\sqrt{(y-\bar{y})^2}_{little}$
LR/NLL2	0.0517	0.2121	0.1468	0.1148	0.2641	0.1477
LR/GR	0.2794	0.0330	0.0538	0.8074	0.4992	0.8415
LR/PS	0.7036	0.2565	0.1936	1.1886	0.5601	1.4504
LR/NLG	0.6888	0.3855	0.4325	0.4362	0.0196	0.1394
NLL1/NLL2	0.0763	0.1664	0.2871	0.2358	0.4825	0.2352
NLL1/GR	0.1591	0.4254	0.3817	1.0289	0.7408	0.4344
NLL1/PS	0.5903	0.1454	0.2681	1.5381	0.8177	1.0266
NLL1/NLG	0.5756	0.0024	0.0018	0.6210	0.2152	0.2665
NLL2/GR	0.2308	0.2512	0.0956	0.7704	0.2341	0.7118
NLL2/PS	0.6580	0.0310	0.0379	1.2091	0.2873	1.3387
NLL2/NLG	0.6432	0.1670	0.2925	0.3575	0.2431	0.0182
GR/PS	0.4119	0.3003	0.1403	0.3171	0.0461	0.6370
GR/NLG	0.3987	0.4313	0.3885	0.4533	0.4766	0.7803
PS/NLG	0.0114	0.1458	0.2739	0.8668	0.5365	1.4519

Table 7: Values of the Student variable, T^*, for tests performed on each pair of registration methods (LR, NLL1, NLL2, GR, PS and NLG) with respect to the variables: $\sqrt{(x-\bar{x})^2}$ and $\sqrt{(y-\bar{y})^2}$ (for thumb, index, little finger samples). Given two samples of size n and having empirical means $\bar{x}_1$ and $\bar{x}_2$, and empirical variances σ_1^2 and σ_2^2, then $T^* = T^*_{2(n-1)} = \frac{\bar{x}_1 - \bar{x}_2}{\sqrt{(\sigma_1^2+\sigma_2^2)}}\sqrt{(n-1)}$; and these two samples are significantly different if $T*^{>}T_{28}$ with $T_{28} = 2.048$ at $\alpha = 0.05$ and $T_{28} = 1.701$ at $\alpha = 0.1$.

on the location of the anatomical points AC-PC). To enlighten the significant difference observed between global methods and method NLL we may note that global methods GR, PS and NLG rely more on luminance information than on anatomical information, whereas the NLL method is fully based on anatomical constraints. That point is a motivation to introduce local anatomical constraints in global registration process [4], [10].

4 Conclusion

We have proposed an inter-individual functional mapping scheme based on the assumption that the inter-subject functional variability is partly encoded in the anatomical variability. Thus the method relies on the modeling of anatomical deformations and on a consistent way to extend them in the vicinity of their initial support. We have modeled the cortical anatomical deformations by building a shape model of cortical sulci via a statistical analysis on a training set. This model provides a compact and precise description of sulci shape and of their variations. Moreover it is independent from a reference subject, since it is relative to a local coordinate system linked to a mean shape. We have proposed an original and consistent framework to extend the matching of cortical sulci in the vicinity of the sulci, thus enabling to merge functional activations, in MEG dipoles form, in this single local coordinate system. This local and non-linear fusion scheme, based on relevant anatomical features, has proven to reduce the inter-subject functional variability. Furthermore, significant difference between this approach and the global methods we presented have been shown. At last, but not least, the registration framework presented here is general and not restricted to MEG activities.

5 Acknowledgments

The authors would like to thank the Brittany Country Council for a contribution to student's grant, and the GIS project (cognition science), as well as the Radiology Department of Pontchaillou hospital in Rennes for data acquisition, and more particularly J-M Scarabin, P. Toulouse and E. Le Rumeur.

References

[1] F. Bookstein. Principal warps: thin-plate splines and the decomposition of deformations. *IEEE Trans. on Pattern Analysis and Machine Intelligence*, 11(6):567–585, 1989.

[2] F.L. Bookstein and D.K. Green. A feature space for derivatives of deformations. In *Proc. Information Processing in Medical Imaging*, volume 687 of *Lecture Notes in Computer*, pages 1–16, 1993.

[3] A. Collignon, D. Vandermeulen, P. Suetens, and G. Marchal. 3d multi-modality medical image registration using feature space clustering. In *Proc. of Computer Vision, Virtual Reality and Robotics in Medicine*, pages 195–204, Nice, France, 1995.

[4] L. Collins, G. Le Goualher, R. Venugopal, A. Caramanos, A. Evans, and C. Barillot. Cortical constraints for non-linear cortical registration. In *Proc. Visualization in Biomedical Computing*, volume 1131 of *Lecture Notes in Computer Science*, pages 307–316, 1996.

[5] T.F. Cootes, C.J. Taylor, D.H. Cooper, and J. Graham. Active shape models - their training and application. *Computer Vision and Image Understanding*, 61(1):38–59, 1995.

[6] J. Duchon. Interpolation des fonctions de deux variables suivant le principe de la flexion des plaques minces. *RAIRO Analyse Numérique*, 10:5–12, 1976.

[7] A. Evans, L. Collins, and B. Milner. An mri-based sterotaxic atlas from 250 young normal subjects. In *Soc. Neuroscience abstract*, volume 18, page 408, 1992.

[8] L. Florack, B. Romeny, J. Koenderink, and M. Viergever. Scale and the differential structures of images. *Image and Vision Computing*, 10:376–388, 1992.

[9] Le Goualher G., E. Procyk, L. Collins, R. Venegopal, Barillot C., and A. Evans. Automated extraction and variability analysis of sulcal neuroanatomy. *IEEE Trans. on Medical Imaging*, 18(3):206–217, 1999.

[10] C. Hellier, P.and Barillot. Cooperation between local and global approaches to register brain images. In *Proc. Information Processing in Medical Imaging*, volume 2082 of *Lecture Notes in Computer Science*, pages 315–328, 2001.

[11] P. Hellier, C. Barillot, I. Corouge, B. Gibaud, G. Le Goualher, D.L. Collins, A. Evans, G. Malandain, and N. Ayache. Retrospective evaluation of inter-subject brain registration. In W. Niessen and M. Viergever, editors, *Proc. Medical Image Computing and Computer Assisted Intervention*, volume 2208 of *Lecture Notes in Computer Science*, pages 258–265, Utrecht, The Netherlands, 2001. Springer-Verlag.

[12] P. Hellier, C. Barillot, E. Mémin, and P. Pérez. Hierarchical estimation of a dense deformation field for 3d robust registration. *IEEE Trans. on Medical Imaging*, 20(5):388–402, 2001.

[13] C. Kervrann and F. Heitz. A hierarchical statistical framework for the segmentation of deformable objects in image sequences. In *IEEE Computer Vision Pattern Recognition*, pages 724–728, 1994.

[14] F. Lachmann and C. Barillot. Brain tissue classification from mri data by means of texture analysis. In *Proc. of SPIE Medical Imaging:Image Processing*, volume 1652, pages 72–83, 1992.

[15] G. Le Goualher, C. Barillot, and Y. Bizais. Modeling cortical sulci with active ribbons. *International Journal of Pattern Recognition and Artificial Intelligence*, 8(11):1295–1315, 1997.

[16] J.B.A. Maintz and M.A. Viergever. A survey of medical image registration. *Medical Image Analysis*, 2(1):1–36, 1998.

[17] J. Martin, A. Pentland, S. Sclaroff, and R. Kikinis. Characterization of neuropathological shape deformations. *IEEE Trans. on Pattern Analysis and Machine Intelligence*, 20(2):97–112, 1998.

[18] J. Mazziotta, A. Toga, A. Evans, P. Fox, and J. Lancaster. A probabilistic atlas of human brain: theory and rationale for its development. *NeuroImage*, 2:89–101, 1995.

[19] T. McInerney and D. Terzopoulos. Deformable models in medical image analysis: a survey. *Medical Image Analysis*, 1(2):91–108, 1996.

[20] K. Rohr, H.S. Stiehl, R. Sprengel, W. Beil, T.M. Buzug, J. Weese, and M.H. Kuhn. Point-based elastic registration of medical image data using approximating thin-plate splines. In *Proc. of Visualization in Biomedical Computing*, pages 297–306, 1996.

[21] D. Schwartz, J.M. Badier, P. Bihoué, and A. Bouliou. Evaluation with realistic sources of a new meg-eeg spatio-temporal localization approach. *Brain Topography*, 11(4):279–289, 1999.

[22] D. Schwartz, D. Lemoine, E. Poiseau, and C. Barillot. Registration of meg/eeg data with 3d mri: methodology and precision issues. *Brain Topography*, 9(2):101–116, 1996.

[23] G. Subsol, J.P. Thirion, and N. Ayache. A general scheme for automatically building 3d morphometric anatomical atlases: application to a skull atlas. *Medical Image Analysis*, 2(1):37–60, 1998.

[24] J. Talairach and P. Tournoux. *Co-planar stereotaxic atlas of the human brain.* Georg Thieme Verlag, Stuttgart, 1988.

[25] A.W. Toga, A. Coldkorn, K. Ambach, K. Chao, B.C. Quinn, and P. Yao. Postmortem cryosectioning as an anatomic reference for human brain mapping. *Computerized Medical Imaging and Graphics*, 21(2):131–141, 1997.

[26] P. Viola and W. Wells. Alignment by maximization of mutual information. In *Proc. Int. Conf. Computer Vision*, pages 15–23, 1995.

[27] W.I. Welker. Why does the cerebellar cortex fissure and fold? a review of determinants of gyri and sulci. In *Comparative Structure and Evolution of Cerebral Cortex*, volume 8, chapter 10, pages 3–136. 1990.

Unité de recherche INRIA Lorraine, Technopôle de Nancy-Brabois, Campus scientifique,
615 rue du Jardin Botanique, BP 101, 54600 VILLERS LÈS NANCY
Unité de recherche INRIA Rennes, Irisa, Campus universitaire de Beaulieu, 35042 RENNES Cedex
Unité de recherche INRIA Rhône-Alpes, 655, avenue de l'Europe, 38330 MONTBONNOT ST MARTIN
Unité de recherche INRIA Rocquencourt, Domaine de Voluceau, Rocquencourt, BP 105, 78153 LE CHESNAY Cedex
Unité de recherche INRIA Sophia-Antipolis, 2004 route des Lucioles, BP 93, 06902 SOPHIA-ANTIPOLIS Cedex

Éditeur
INRIA, Domaine de Voluceau, Rocquencourt, BP 105, 78153 LE CHESNAY Cedex (France)
http://www.inria.fr
ISSN 0249-6399